The Role of Turbulent Mixing in an Overturning Circulation Maintained by Surface Buoyancy Forcing

KIAL D. STEWART, GRAHAM O. HUGHES, AND ROSS W. GRIFFITHS

The Australian National University, Canberra, Australian Capital Territory, Australia

(Manuscript received 27 December 2011, in final form 21 May 2012)

ABSTRACT

The role of externally imposed rates of small-scale mixing in an overturning circulation forced by differential surface buoyancy fluxes is examined in a laboratory experiment. The circulation occupies the full volume and involves a dense turbulent plume against the endwall and a broad upwelling throughout the interior. For strong externally imposed stirring, turbulent diffusion is the primary means of vertical density transport in the flow, and the dependence of the equilibrated circulation on the mixing rate accords with a theoretical model; the overturning rate increases as the $^1/_4$ power of the turbulent diffusivity. For weak externally imposed stirring, advection is the dominant mechanism of vertical density transport, and the circulation is independent of the rate of external stirring. The rate of vertical density transport is parameterized as a bulk diffusivity obtained from different methods, including one from a Munk-like advection–diffusion balance and another from the transport of buoyancy across the surface. For strong stirring, the bulk diffusivities returned by the various methods agree with the externally imposed mixing rate. However, the parameterizations implicitly include a nondiffusive component of vertical transport associated with advection of the density field and it is shown that, for weak stirring, the bulk diffusivities exceed the externally imposed mixing rate. For the oceans, results suggest that the primary effect of mixing (with energy sourced from winds, tides, and convection) is to deepen the thermocline, thereby influencing the entrainment and consequent vertical transport of density in the dense sinking regions. It is concluded that this advective transport of density, and not vertical mixing, is crucial for coupling the surface to the abyss.

1. Introduction

The meridional overturning circulation (MOC) of the global oceans is inextricably linked to vertical mixing in its interior (Munk 1966; Munk and Wunsch 1998; Kuhlbrodt et al. 2007). The circulation involves poleward transport of heat in the thermocline, the formation of dense waters at high latitudes, the sinking of these dense waters to abyssal depths, and a return flow of some form equatorward and upward. There are two forces available to drive this large-scale circulation: surface wind stress and buoyancy. The relative roles of these forces, whether heat transport is passive and wind stress is dominant (Wunsch and Ferrari 2004) or whether buoyancy can be significant (Hughes and Griffiths 2006), remains under debate. However, it is clear that the latitudinal gradient of surface buoyancy fluxes is essential in maintaining the global density stratification. The sinking of dense water (as overflows and gravity currents) refills the deep ocean basins, maintaining the top-to-bottom density difference. At the same time, the MOC and the observed density stratification can coexist only if there is a continual downgradient diffusive transport of density. Stronger vertical mixing tends to reduce the vertical density gradient and lead to a more rapid MOC (see e.g., Bryan 1987; Hughes and Griffiths 2006). However, a detailed physical understanding of the coupling between mixing and the MOC is yet to emerge.

Here we use laboratory experiments to investigate the dependence of overturning rate on the rate of imposed mixing in a convective circulation. The experiment is forced by differential surface buoyancy fluxes (salt and freshwater), and the rates of mechanical stirring imposed throughout the flow are varied to give vertical diffusivities that span four orders of magnitude. Mean flows driven by wind stress and Ekman pumping are not represented so as to focus on the relationship between the circulation

Corresponding author address: K. D. Stewart, Research School of Earth Sciences, The Australian National University, Mills Road, Acton ACT 0200, Australia.
E-mail: kial.stewart@anu.edu.au

DOI: 10.1175/JPO-D-11-0242.1

and turbulent mixing. A more detailed discussion of background material is given in section 2, the experimental setup and method are described in section 3, the results are reported in section 4, and a discussion of significant points is presented in section 5.

2. Background

An understanding of the behavior of the convective circulation forced by differential surface buoyancy fluxes, often referred to as ''horizontal convection,'' is still developing (Hughes and Griffiths 2008). The form of the buoyancy-driven circulation, as first shown experimentally by Rossby (1965), includes a boundary layer adjacent to the horizontal boundary at which the buoyancy fluxes occur (i.e., the surface in the case of the oceans). The boundary layer, or thermocline, is a strongly stratified region, particularly where the surface buoyancy flux is stabilizing. Horizontal flow in the boundary layer carries water toward the region of destabilizing surface buoyancy flux. Waters that become sufficiently dense there feed into a sinking plume. For large Rayleigh numbers (defined below) this plume is turbulent and entrains water during its descent (Mullarney et al. 2004; Whitehead and Wang 2008). Hence the typical top-to-bottom density difference in the system can be substantially less than the range of surface densities. Entrainment also causes the plume to contribute to the maintenance of a stable stratification throughout the domain outside the plume (Hughes and Griffiths 2006). In a stationary state (the large-time equilibrium), there can be no net (time-averaged) buoyancy flux through any level (including the surface, Paparella and Young 2002).

Ocean general circulation models, such as those of Bryan (1987) and Tsujino et al. (2000), show an overturning circulation with a number of features reminiscent of horizontal convection. They also predict a rate of meridional overturning that increases with the value of interior vertical diffusivity κ_{TOT}, which represents the rate of vertical (or diapycnal) transport due to unresolved subgrid-scale processes in the model, such as small-scale turbulence. The effect of changing this diffusivity in the models was in line with the theory that the abyssal circulation is governed by a vertical advection–diffusion balance (Munk 1966), and there was consistency in the order of magnitude of the diffusivity (10^2 to 10^3 times the molecular value for heat) required to support the observed rate of overturning.

Numerical simulations (Mullarney et al. 2004) have since provided two-dimensional solutions for horizontal convection under conditions typical of laboratory experiments in which horizontal differences in temperature or heat flux were applied to achieve moderately large Rayleigh numbers [$O(10^{12})$ based on the horizontal temperature difference]. Unlike general circulation models, these simulations did not attempt to mimic additional external mechanical forcing of turbulent mixing, and a range of small-scale flow instabilities occur without the hydrostatic approximation and the parameterization of the vertical convective motions required in the ocean models. Comparison of the numerical simulations with an analytical model (Hughes et al. 2007), in terms of the Nusselt number and boundary layer thickness, provides evidence that under the simulated conditions the effective interior diffusivity κ_* remained comparable to (but possibly a few times larger than) the molecular diffusivity κ_m. For large Rayleigh numbers, Paparella and Young (2002) obtained an upper bound on the volume-averaged turbulent dissipation rate for kinetic energy that has been interpreted to mean that the accompanying interior mixing remains weak for a circulation forced by surface buoyancy fluxes alone. However, a statistical analysis of the velocity field of 3D direct numerical simulations of horizontal convection suggests that surface buoyancy forcing can support turbulent motions that contribute significantly to interior vertical mixing rates, which are not closely coupled to the dissipation rate (Scotti and White 2011).

The oceans therefore contain numerous sources of energy that may contribute to small-scale turbulence and consequent irreversible vertical mixing. Hence, it is important to understand the implications of additional mixing and at what levels it has significant effects. It is the total vertical transport of density (including any externally energized component of irreversible mixing) that is routinely parameterized by the diffusivity κ_{TOT} in numerical models (see discussion in Hughes et al. 2009). Similarly, the effective interior diffusivity κ_* in the theoretical model of Hughes and Griffiths (2006) does not distinguish between mixing owing to molecular diffusion down the mean gradient and those gradients promoted by turbulent stirring, or between mixing attributable to convective stirring and that generated by other forcing. One could in principle carry out thermal convection experiments in the laboratory (such as those referred to above), with some form of additional mechanically induced mixing. However, thermally forced experiments have three practical limitations: the experimental ocean basin cannot be perfectly insulated to prevent heat gain or loss, temperature provides only a small dynamical range of densities or buoyancy fluxes, and heat has a relatively large molecular diffusion coefficient when working at the laboratory scale. In this study we turn to salt to provide a solutal buoyancy forcing, allowing conservation of buoyancy, a larger dynamical range of densities, and a molecular diffusivity small

enough to allow the transport to be determined by mechanical stirring.

Salinity differences have previously been used to study the convective flow that arises from surface fluxes of fresh and saline water located at opposite ends of a rectangular tank, with a forced sink situated between the sources to maintain an approximately constant volume (Pierce and Rhines 1996). Although these experiments did not reach a stationary state, they revealed a deep circulation and a thin surface boundary layer, similar to the previous experiments examining horizontal convection. Whitehead and Wang (2008) extended the experiments of Pierce and Rhines (1996) by replacing the forced sink with a passive spillway at the surface and using a vertical rod to introduce turbulent mixing to the circulation. The source and spillway configuration ensured that the volume of the tank was constant at all times, and the experiments were reported to have run long enough to reach an equilibrated state under the imposed density boundary conditions. Those experiments showed that the additional turbulent mixing deepened the surface boundary layer and reduced the average density in the tank. However, a comparison cannot be made with existing theory because no metric was provided for the amount of turbulent mixing generated by the stirring rod and the overturning rate was not measured. Additionally, the source and sink (or spillway) arrangement in both of the above experiments imposed serious constraints on the density within the circulation at the depth of the sink or spillway because the density of the water exiting the sink in steady state had to be the average of the fresh and saline source waters.

The dimensionless parameters describing the equilibrium state of the flow in a simple rectangular domain, when forced purely by surface buoyancy conditions, are the flux Rayleigh number

$$\mathrm{Ra}_B = \frac{BL^3}{\nu_m \kappa_m^2}, \tag{1}$$

the Prandtl (or Schmidt) number of the fluid

$$\mathrm{Pr} = \frac{\nu_m}{\kappa_m}, \tag{2}$$

and the aspect ratio of the domain

$$A = \frac{D}{L}, \tag{3}$$

where B ($\mathrm{m^3\ s^{-3}}$) is the specific buoyancy flux per unit (spanwise) width, ν_m ($\mathrm{m^2\ s^{-1}}$) is the kinematic viscosity of the fluid, κ_m ($\mathrm{m^2\ s^{-1}}$) is the molecular diffusivity of the stratifying species (e.g., heat or salt), and D (m) and L (m) are the depth and length of the domain, respectively. The flux Rayleigh number divided by the appropriate Nusselt number ($\mathrm{Nu} = B/\kappa_m g'$) gives the usual Rayleigh number ($\mathrm{Ra} = g' L^3/\nu_m \kappa_m$), where g' is the reduced gravity based on the density contrast between sources that are separated horizontally by a length scale $O(L)$. It is important to note that we choose here to define the governing parameters in terms of the molecular fluid properties that are known a priori. However, when additional stirring is included in the problem, two further variables are required and we express these as the effective (turbulent) diffusivity and viscosity, for which the governing parameters are κ_*/κ_m and ν_*/ν_m, respectively.

A scaling analysis for the circulation within a viscous boundary layer and forced by an imposed buoyancy flux in a basin of rectangular surface area (Mullarney et al. 2004, following Rossby 1965) gives the boundary layer thickness δ normalized by L as,

$$\frac{\delta}{L} \sim \mathrm{Ra}_B^{-1/6} \left[= \left(\frac{BL^3}{\nu_m \kappa_m^2} \right)^{-1/6} \right]. \tag{4}$$

For a given buoyancy flux and basin length (4) predicts that the boundary layer thickness depends on viscosity and diffusivity as

$$\delta \sim \nu_m^{1/6} \kappa_m^{1/3}. \tag{5}$$

In a very different approach, Hughes et al. (2007) obtained a closed solution for flow at large Rayleigh numbers by coupling the equations describing a turbulent plume to those for the transport of density by advection and diffusion in the interior of the basin. In this inviscid solution the Prandtl and Rayleigh numbers appear only as their product, removing all dependence on the viscosity. Furthermore, it was assumed that the relevant diffusivity in such a formulation would be the effective diffusivity κ_* for density resulting from both molecular diffusion (down the mean gradient) and that promoted by stirring in the interior. For the case of a rectangular basin (which has a plume descending from a two-dimensional line source with an entrainment coefficient of 0.1, e.g., Turner 1986) this solution gives the boundary layer thickness as

$$\frac{\delta}{L} = 3.95\, \mathrm{Pr}_*^{-1/6}\, \mathrm{Ra}_{B*}^{-1/6} \left[= 3.95 \left(\frac{\nu_*}{\kappa_*} \right)^{-1/6} \left(\frac{BL^3}{\nu_* \kappa_*^2} \right)^{-1/6} \right], \tag{6}$$

where Ra_{B*} and Pr_* are defined in terms of the effective turbulent diffusivity and viscosity, and the constant is evaluated for a boundary layer thickness that

incorporates 95% of the top-to-bottom density difference. In this case, again holding the buoyancy flux fixed,

$$\delta \sim \kappa_*^{1/2}. \tag{7}$$

The effective interior diffusivity (and viscosity) would reduce to the molecular value at sufficiently small Rayleigh numbers and no externally imposed mechanical mixing. The results (5) and (7) are then reconciled for a constant (turbulent) Prandtl number, such that $\nu_* \sim \kappa_*$, in which case (5) reduces to (7). Hughes et al. (2007) argued that viscosity is ineffective on the large length scales of the interior and hypothesized that at high Rayleigh numbers the flow in the boundary layer, even if it is viscous, is set by the interior flow. [We note that when holding g' fixed in both the Rossby (1965) scaling and the inviscid model, the boundary layer scales as $\delta \sim \kappa_*^{2/5}$.]

Hughes et al. (2007) also predicts the horizontally averaged top-to-bottom density difference $\Delta\rho_V$ and streamfunction maximum $\Psi_{\max}$ to vary with κ_* (for fixed B) as

$$\Delta\rho_V \sim \kappa_*^{-1/2}; \quad \Psi_{\max} \sim \kappa_*^{1/4}. \tag{8}$$

This solution was tested using experiments and numerical simulations of thermal convection in which the heat input was varied (and assuming $\kappa_* = \kappa_m$), with good agreement found for the Nusselt number–Rayleigh number relation and the dimensionless boundary layer thickness (6). However, the dependence on diffusivity has not been tested explicitly.

In the experiments reported here we investigate the rate of overturning for a range of known vertical diffusivities. This study does not focus on the energetics of the overturning, rather we aim to obtain a clear picture of the dynamics of the flow. Although these buoyancy-driven overturning circulations cannot be considered pure horizontal convection (for reasons detailed later), they provide an opportunity to compare measurements of the convective circulations with the theoretical predictions of Hughes et al. and to examine how the density field and flow (arising from imposed flux boundary conditions) vary with the level of turbulent mixing. The results also allow an examination of the nature of the vertical mixing rates obtained from the Munk (1966) abyssal recipe.

3. Experiments

a. Apparatus

The convection experiments were performed in an acrylic tank with internal dimensions of length, depth, and width 1.2 m × 0.6 m × 0.08 m (Fig. 1); a vertical partition wall was inserted such that the model basin in which the overturning circulation was confined (and which will be referred to as the ''working volume'') was 1.16 m × 0.53 m × 0.08 m ($L \times D \times W$, respectively). Thus the aspect ratio was fixed at $A = 0.457$. Fresh and saline water were gravity fed from two constant-head supplies to the upper right- and left-hand ends of the working volume, respectively. The vertical partition at the left-hand end allowed an overflow at the top, thus maintaining a constant working volume. The experiments were carried out in a laboratory held at 20 ± 1°C and all water entering the tank was previously equilibrated to the laboratory temperature. The tank was also insulated on all sides by 30 mm of expanded polystyrene foam board; this was removed only for short periods for flow visualization.

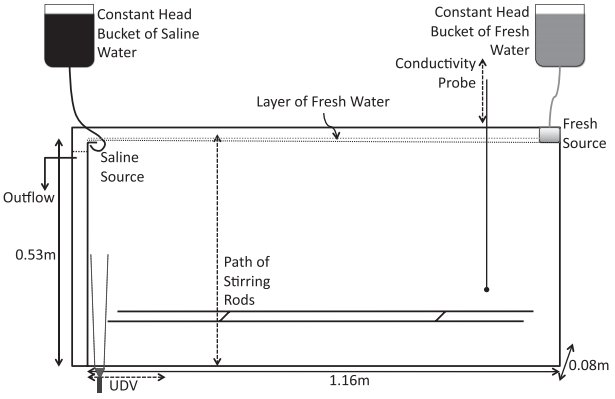

FIG. 1. Schematic drawing of the experimental setup for expts 1–9 (for expts 10 and 11 the saline source is located at the bottom left-hand corner of the tank). Freshwater in the layer above the working volume is (top right) continuously renewed from the source and (top left) exits the tank after passing across the overflow. The saline water source is injected at the top-left corner as a turbulent plume that sinks to the bottom of the tank. Ultrasonic Doppler Velocity measurements using a vertical beam were taken at discrete locations in the range shown by the dashed horizontal arrow. The stirring rods repeatedly traversed the full-depth of the water column. The conductivity–temperature probe was profiled vertically at a fixed horizontal position.

In a separate, well-mixed and insulated reservoir 400 L of saline water were prepared. This saline water was continuously recycled through one of the constant-head supplies from which a portion of the same saline water was gravity fed into the tank via a small tube at a constant rate. Injection of momentum to the circulation was avoided by directing the outlet of the small tube upward into the upper left-hand corner of the working volume, where a small ''lip'' acted to distribute the saline water across the tank width. This lip also physically separated the saline water from the overflow, preventing

the immediate escape of saline water from the working volume. Thus, the source of saline water effectively gave rise to a full-width (line) endwall plume (with no initial vertical momentum), which was turbulent at all levels below the upper corner of the working volume. The volume flux (per unit tank width) and the density of the saline source were held constant for all experiments at $Q_s = 35.42$ mm^2 s^{-1} and $\rho_s \approx 1022$ kg m^{-3} (salinity $S_s \approx 0.034$ kg kg^{-1}), respectively, thus imposing the specific buoyancy flux (per unit tank width),

$$B = g\beta(S_s - S_f)Q_s, \tag{9}$$

supplied to the tank. The coefficient of expansion β for salt has the value 0.69 and, with the salinity of freshwater $S_f = 0$, substituting (9) into (1) gives a flux Rayleigh number $\mathrm{Ra}_B = 5.7 \times 10^{18}$ for the experiments. The salt diffusivity is $\kappa_m = 1.39 \times 10^{-9}$ m^2 s^{-1} and the Prandtl (Schmidt) number (2) is Pr = 671 (Washburn 2003).

A 200 L reservoir of freshwater ($\rho_f \approx 998.3$ kg m^{-3}) was maintained at constant volume by a ballcock set plumbed to the filtered mains water supply. This water was continuously recycled through the second constant-head supply from which a portion was gravity fed to the tank, via a small tube, at a constant rate. The freshwater entered at the free surface through a small chamber that had a porous base designed to remove any input momentum, create a smooth outflow, and maintain an overlying layer of freshwater; the volume flux per unit tank width was $Q_f = 83.33$ mm^2 s^{-1}. The freshwater flowed along the length of the tank and exited in the overflow above the partition wall. The interface between this layer of freshwater and the underlying denser waters defined the upper surface of the working volume. The boundary condition at the upper surface was therefore a constant and uniform density, corresponding to freshwater. Unlike the injection of saline water into the working volume, the vertical volume flux of freshwater across the upper surface was not imposed, rather it was free to adjust to that required by the internal dynamics of the circulation. The vertical transport of salt, on the other hand, across the upper surface must equal the source input, and the salinity is not constrained anywhere excepting at the source and at the surface, where $S = 0$. [The latter condition is in contrast to that achieved in Whitehead and Wang (2008).] We note that the shear stress applied along the upper surface by the fresh layer had a negligible effect on the circulation (as demonstrated by additional experiments in which the direction of flow of the fresh layer was reversed). Moreover, no direct mixing across the interface was detectable—the local Richardson number was estimated to be larger than $O(10)$ in all cases.

Profiles of salinity/density were measured through the depth of an experiment using a PME MicroScale Conductivity and Temperature probe (Model 125) mounted to a computer-controlled traversing mechanism. The conductivity probe was calibrated before each profile and a few small-volume water samples were withdrawn during each profile to enable the calibration accuracy to be monitored (see §3.c). The probe was immersed in the freshwater layer when not in use.

Vertical velocities in the sinking plume were measured using a *Signal Processing* 8 MHz Ultrasonic Doppler Velocimeter (UDV) transducer (Model DOP2000) directed upward from underneath the left-hand end of the tank. The transducer could be translated horizontally along one quarter of the tank length, and was acoustically coupled with the acrylic base through a thin gel layer. Good-quality velocity data were obtained by preseeding the circulation in the tank with near neutrally buoyant Pliolite particles (70–125 μm diameter, which were prewetted in the salt source solution of density ρ_s). The vertical component of velocity was obtained at 240 intervals along the vertical beam line to a distance 180 mm above the base at 0.5 s intervals.

b. Mechanical stirring

Mechanical agitation was generated in the flow (in addition to the stirring associated with the convection) by a pair of coplanar horizontal rods that were oscillated while continuously traversing through the full depth of the tank. The rods were stainless steel, each 1.12 m in length and $l = 8$ mm in diameter, with their axes separated by two 32 mm struts and extending along the length of the tank. Small spacers ensured that the rods remained parallel to and equidistant from the sidewalls. The rods were suspended by stainless steel wires (diameter 0.02 mm) from a frame above the tank. This frame was driven by a computer-controlled *Animatics* "SmartMotor" such that the vertical velocity of the rods consisted of a constant mean (traversing) component ($\overline{V}$, alternately upward or downward between reversal points at the top and bottom) and a relatively high frequency sinusoidal fluctuation (V'), both of which are proportional to the angular velocity of the motor ω (varied over the range $\omega = 0$ to 13.1 rad s^{-1}). The vertical velocity (mm s^{-1}) of the rods can be described as

$$V(\omega, t) = \overline{V}(\omega) + V'(\omega, t) = \frac{6\omega}{\pi} + 12\omega \sin(\omega t). \tag{10}$$

The turbulent eddies generated by the rods are therefore expected to have a length scale l, and this complicated motion was designed to prevent advection of tracer in the rod wake over large vertical distances, such

that the consequent mixing can be represented as a Fickian diffusion process. The time taken for the stirring rods to pass through the depth ranged from 14 to 189 s (infinite for $\omega = 0$), with the associated periods of oscillation ranging from 0.48 to 6.71 s (also infinite for $\omega = 0$). Uniform stirring was imposed throughout the working volume and the time between stirring events was much less than the overturning time scale of the circulation ($\sim 2 \times 10^3$ s). Active stirring at any given location occurred for the fraction $3l/D \approx 0.045$ of the total time (an intermittency coincidently similar to that in the ocean thermocline, Gregg 1987).

The overall effect of the rods was to introduce small-scale three-dimensional motions that stirred the density field, causing irreversible diapycnal mixing. The time-averaged rate of mixing was measured for each level of stirring in calibration experiments starting with a two-layer stratification (freshwater overlying saline water) and conducted in the same apparatus as the actual experiments. A known quantity of passive dye tracer was added initially to the saline water and the subsequent evolution of the concentration field was measured optically. Light passing through the flow was attenuated by an amount dependent upon the local dye concentration, and a high-resolution digital camera was used to measure the relative attenuation field at many times during each calibration experiment [which lasted $O(100)$ traverses of the stirring rods]. The normalized and horizontally averaged dye (or salt) concentration profile $C'(z, t)$ was calculated from the relative attenuation field at each time t and fitted to the solution for Fickian diffusion:

$$C'(z,t) = \mathrm{erf}\left(\frac{z}{2\sqrt{\kappa_E t}}\right), \tag{11}$$

where depth z is measured relative to the initial interface position and κ_E is the (best-fit) diffusivity. The profiles were accurately described by the error function and Fig. 2 shows the diffusivities obtained. Over the range $\kappa_E \approx O(10^{-9}$–$10^{-5})$ m^2 s^{-1} the diffusivities are well described by the empirical relationship $\kappa_E = 0.027\overline{V}^{2.5}$. The best-fit diffusivity $\kappa_E = 2.67 \times 10^{-9}$ m^2 s^{-1} measured for $\overline{V} = 0$ is a factor of 2 larger than the accepted coefficient of molecular diffusion ($\kappa_m = 1.39 \times 10^{-9}$ m^2 s^{-1}, Washburn 2003) for NaCl in water at 20°C; the difference is likely to be a consequence of additional convective transport arising from imperfect insulation during the $\sim$24 h calibration run. Although the case with no additional mechanical stirring anchors the calibration results, the contribution to the total vertical salt transport of molecular diffusion down the mean gradient is expected to be negligible at the nonzero stirring rod speeds used.

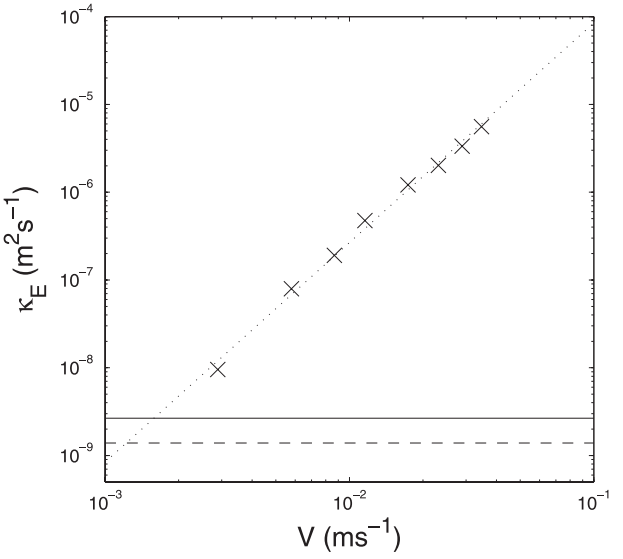

FIG. 2. Plot of κ_E as a function of $\overline{V}$: the solid line is the calibrated value of κ_E for $\overline{V} = 0$ (i.e., no rod stirring), and the dashed line shows the accepted value for molecular diffusion of salt in water, $\kappa_m = 1.39 \times 10^{-9}$ m^2 s^{-1} (Washburn 2003). The least squares fit, shown by the dotted line, is that of the relationship $\kappa_E = 0.027\overline{V}^{2.5}$.

Thus, the product of κ_E and the local density gradient is proportional to the density flux due to the externally imposed stirring. Hence, κ_E will be referred to here as the externally imposed diffusivity while recalling that it also includes the component of transport due to molecular diffusion down the mean gradient and approaches κ_m when there is no mechanically induced mixing. No physical argument is offered for the particular functional relationship between κ_E and $\overline{V}$ found here, which may be valid only for the present apparatus and stirring style. The motion of the stirring rods was particularly violent for $\overline{V} > 34.7$ mm s^{-1} and a good fit to (11) was not possible; we take this traversing velocity as the upper limit for which the apparatus and method are useful.

c. Method and measurements

The working volume was filled with freshwater. The freshwater source, stirring rods, and saline water source were then switched on, and the experiment left to come to equilibrium—a stationary state in which there was zero net buoyancy/salt flux into the experiment. A conservative estimate of the time scale required to approach equilibrium is provided by the "filling time scale" [i.e., the time required for the saline source to replace the tank volume, $Q_s/(L \times D) \approx 2 \times 10^4$ s]; in practice, the adjustment to equilibrium was more accurately represented by the overturning time scale [$\Psi_{\max}/(L \times D) \approx 2 \times 10^3$ s], however, this was not known a priori. Nevertheless, each experiment was run for 5–6 filling time scales (25–30 h)

before detailed measurements were carried out. Monitoring of the overflow salinity was used to verify equilibration of the experiment. Conservation of volume and salt requires the overflow to have the volume transport

$$Q_o = Q_s + Q_f, \tag{12}$$

and hence the equilibrium salinity

$$S_o^* = \frac{Q_s S_s + Q_f S_f}{Q_o} = \frac{Q_s S_s}{Q_s + Q_f}. \tag{13}$$

It is worth noting that the overflow in these experiments does not have the effect of the sink or spillway used in previous studies (Pierce and Rhines 1996; Whitehead and Wang 2008), where water was withdrawn directly from the working volume, therefore participating in the circulation. Here the large throughput of freshwater keeps the upper boundary condition as fresh and the overflowing layer accommodates the salt leaving the working volume.

After the equilibrium state was reached, a profile of conductivity and temperature was measured through the depth of the tank 0.17 m from the right-hand endwall, which was chosen as a location representative of the interior. The conductivity–temperature probe was traversed with a velocity and sampling rate that gave a vertical resolution of 0.625 mm. Immediately following each profile three standard solutions were used to check the conductivity probe calibration. In addition, 3-ml water samples were taken at depths of 0, 20, and 200 mm below the top of the working volume and in the same horizontal location as the profile. The densities of the standards, samples, sources and outflow were measured to an accuracy of 5 parts in 10^7 in an Anton–Paar precision densimeter (Model DMA5000) and used in conjunction with the conductivity data (Ruddick and Shirtcliffe 1979) to produce each vertical profile of density. The effect on density of temperature variations throughout the depth (and across all experiments) of less than 1°C were negligible compared with that due to salinity variations. To check the stability of the equilibrium state, the profiling and sampling procedure was carried out twice for each experiment, separated by at least one filling time scale (~6 h).

Between conductivity profiles the saline water source was seeded with particles for UDV measurements. Profiles of vertical velocity above the base of the tank were constructed at seven locations 20 mm apart, between 12 and 152 mm from the left-hand end of the working volume. At each location more than 500 individual profiles were recorded over a duration of approximately four minutes. Both spikes and null readings were first removed from these profiles, which were then averaged to give a single profile for each location, which was relatively insensitive to perturbations introduced by passage of the stirring rods. The mean vertical velocity was integrated horizontally from the endwall to the position where the vertical velocity changed sign (thus defining the outer edge of the plume), giving the streamfunction in the plume as a function of position. Its maximum value, $\Psi_{\max}$ ($\mathrm{mm^2\ s^{-1}}$), occurred near the top of the plume outflow along the base of the tank, and this is taken as the maximum streamfunction value for the circulation.

Eleven experiments are reported here (Table 1); in nine of these only the mechanical stirring was varied. In two further runs (experiments 10 and 11) the turbulent plume was eliminated by relocating the saline source to the base of the tank. The results are discussed below in terms of the vertical density structure, boundary layer thickness, top-to-bottom density difference, and maximum streamfunction.

4. Results

a. *Qualitative description*

The mechanical stirring in these experiments did not qualitatively alter the large-scale circulation observed previously in horizontal convection experiments (e.g., Rossby 1965; Mullarney et al. 2004). The intermittent passage of the stirring rods excited local three-dimensional turbulence that quickly decayed. The saline source sustained a turbulent line plume that descended against the left-hand endwall (Fig. 3a). The horizontal entrainment velocity into the plume (as indicated by the distortion of initially vertical dye lines generated by dropping $KMnO_4$ crystals through the flow) varied with depth and was largest in the upper one-fifth of the depth. The plume penetrated to the tank bottom only intermittently, as a consequence of large fluctuations induced by the stirring rods throughout the tank. An outflow from the plume was established along the base of the tank (Fig. 3b), with a depth that was approximately one-quarter that of the working volume. The mean shear in the outflow always supported three-dimensional eddies and mixing, but this was less vigorous than in the plume. Water in the outflow tended to continually displace the overlying water column upward (Figs. 3c,d). However, the upwelling decreased toward the surface, as expected for substantial entrainment into the plume at intermediate depths.

b. *Measurements*

The measured profiles of density shown in Fig. 4a are presented in normalized form

TABLE 1. Table of experiments and corresponding measurements; for the experiment numbers (a) and (b) denote the conditions prevailing for the two profiles in each experiment. Quantities are the mean (traversing) velocity $\overline{V}$ of the stirring rods, the "externally imposed" diffusivity κ_E measured in calibration runs, the density difference $\Delta\rho$ between the source waters, the normalized "top-to-bottom" density difference $\Delta\rho_n$, the boundary layer thickness δ, and the maximum streamfunction $\psi_{\max}$ defining the total overturning transport.

Expt	$\overline{V}$ (mm s^{-1})	κ_E (m^2 s^{-1})	$\Delta\rho$ (kg m^{-3})	$\Delta\rho_n$	δ (mm)	$\psi_{\max}$ (mm^2 s^{-1})
1(a)	0	2.67×10^{-9}	24.31	0.99	6.75	216
1(b)	0	2.67×10^{-9}	24.31	0.99	6.45	216
2(a)	2.9	9.57×10^{-9}	23.53	0.99	6.05	247
2(b)	2.9	9.57×10^{-9}	23.53	0.99	5.33	247
3(a)	5.8	7.95×10^{-8}	22.97	0.98	5.90	238
3(b)	5.8	7.95×10^{-8}	22.97	0.98	6.50	238
4(a)	8.7	1.91×10^{-7}	23.90	0.92	7.54	264
4(b)	8.7	1.91×10^{-7}	23.90	0.92	8.00	264
5(a)	11.6	4.76×10^{-7}	23.79	0.86	11.54	318
5(b)	11.6	4.76×10^{-7}	23.79	0.86	11.00	318
6(a)	17.4	1.21×10^{-6}	23.98	0.68	18.52	410
6(b)	17.4	1.21×10^{-6}	23.98	0.69	17.80	410
7(a)	23.1	2.02×10^{-6}	24.11	0.55	20.41	476
7(b)	23.1	2.02×10^{-6}	24.11	0.54	20.04	476
8(a)	28.9	3.35×10^{-6}	24.18	0.42	28.36	538
8(b)	28.9	3.35×10^{-6}	24.18	0.43	35.33	538
9(a)	34.7	5.59×10^{-6}	23.31	0.37	35.50	648
9(b)	34.7	5.59×10^{-6}	23.31	0.35	34.50	648
10	0	2.67×10^{-9}	25.18	1	—	35
11	17.4	1.21×10^{-6}	25.52	1	—	35

$$\rho_n(z) = \frac{\rho(z) - \rho_f}{\Delta\rho}, \tag{14}$$

where $\Delta\rho = \rho_s - \rho_f$ is the maximum density difference (measured between the source water reservoirs) and $\rho(z)$ is the density calculated from the conductivity measured at depth z. The two profiles measured for each experiment are almost coincident (hence only one of these is plotted in Fig. 4a), verifying that the circulation had reached a well-defined equilibrium state. The density structure is similar to that measured in thermally-forced horizontal convection (Rossby 1965; Mullarney et al. 2004) and reveals a strongly stratified boundary layer overlying a weakly stratified interior. As the mechanical stirring increases (with the boundary conditions held fixed) the boundary layer thickens, the water at any given depth freshens, the density gradient is everywhere smaller, and there is a smaller top-to-bottom density difference.

The boundary layer thickness δ is defined here as the depth below the surface that accommodates 92.5% of the top-to-bottom density difference; given the shape of the density profiles, this threshold was chosen to be as large as possible without δ being unduly sensitive to the density fluctuations associated with the turbulence (some of which are just visible in Fig. 4a). Thus δ, normalized by the depth of the working volume D, is plotted in Fig. 4b as a function of the ratio κ_E/κ_m. The data indicates two regimes: the boundary layer thickness δ is independent of the mixing rate κ_E for $\kappa_E/\kappa_m < 10^2$ (termed 'weak stirring') and increases with κ_E for $\kappa_E/\kappa_m > 10^2$ ('strong stirring').

Measurements of the top-to-bottom density difference,

$$\Delta\rho_V = \rho(D) - \rho_f, \tag{15}$$

are presented in normalized form in Fig. 4c as an adjusted salinity difference,

$$\beta\Delta S_n = \frac{\Delta\rho_V}{\rho_f}\frac{\overline{\Delta\rho}}{\Delta\rho}, \tag{16}$$

where $\rho(D)$ is the density measured at the base and $\overline{\Delta\rho}$ is the mean density difference between the sources in experiments 1–9. The adjustment factor $\overline{\Delta\rho}/\Delta\rho$ allows data from experiments with minor differences in source water densities to be rescaled and compared. Two regimes are again evident: $\beta\Delta S_n$ is independent of κ_E for $\kappa_E/\kappa_m < 10^2$ and decreases with κ_E for $\kappa_E/\kappa_m > 10^2$. Note that the bottom density approaches the source density [$\rho_n(D) \to 1$ and $\beta\Delta S_n \to \overline{\Delta\rho}/\rho_f$] when the mixing is weak (Figs. 4a,c). This occurs primarily because the boundary layer becomes thinner as κ_E decreases, reducing the amount of freshwater entrained into the plume and thus carried to

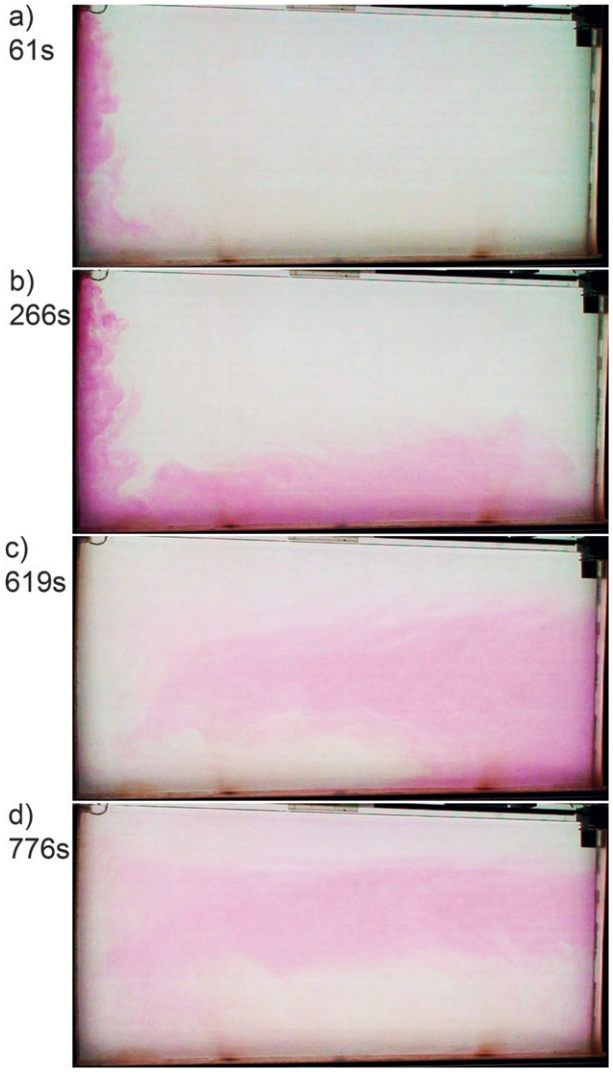

FIG. 3. Photographs showing qualitatively the overturning circulation in expt 1, following a temporary injection of dye between $t = 0$ s and $t = 459$ s via the saline source (upper left). Each frame indicates the relative strength of the flow in different parts of the overturning circulation: (a) the turbulent plume descending the left endwall; (b) the outflow from the plume along the base of the tank; and (c),(d) a relatively dispersed cloud of dye indicates the broad upwelling over time of water in the circulation interior.

depth. The diffusive transport of freshwater to depths below the boundary layer is negligible.

The maximum measured volume transport ($\Psi_{\max}$) in the overturning circulation is shown in Fig. 5, normalized by the volume flux of the saline source. In all cases, entrainment into the plume increases the maximum volume transport to more than $6Q_s$. The two regimes are apparent: volume transport was independent of κ_E for $\kappa_E/\kappa_m < 10^2$, and for $\kappa_E/\kappa_m > 10^2$ the transport increases by approximately threefold when κ_E increases by a factor of 30.

5. Discussion

For sufficiently strong stirring ($\kappa_E/\kappa_m > 10^2$) the experiments recover the dependences on turbulent diffusivity predicted by the model of Hughes et al. (2007) for boundary layer thickness (7), top-to-bottom density difference (8), and total transport (8) (see Figs. 4b,c and 5). The scaling for boundary layer thickness is also consistent with the buoyancy–viscous balance of Rossby (1965) if the molecular properties in (4) are replaced by their turbulent counterparts and $\nu_* \sim \kappa_*$ is assumed (as per the discussion in §3). The constant predicted by Hughes et al. for the boundary layer thickness and the overturning transport is about a factor of 2 greater than that suggested by the measurements. The most likely reasons for this difference are that a marginally greater threshold (95%, which was impractical to use for the experiments) was used to define the boundary layer in the theory and that the saline source does not match an idealized plume source (see below) close to the upper surface—the volume flux in experiments was greater in this region, increasing the local upwelling and acting to thin the boundary layer. A thinner boundary layer is then consistent with a more rapid than predicted decrease with depth of plume buoyancy flux, leading to a smaller overturning transport.

For experiments with weak stirring ($\kappa_E/\kappa_m < 10^2$) the flow and density structure are independent of the externally imposed mixing rate. We suggest that the mismatch with theoretical scaling dependences in this regime is again associated with differences, close to the upper surface, between the assumed plume source and that used in experiments—specifically, that the vertical transport of density near the surface is not dominated by the externally imposed rate of mixing (see below).

Improved physical insight into the observations is generated by applying a ''virtual source'' correction (appendix) to the measurements, allowing wider comparison with theory. The principle behind the correction procedure is that a buoyancy source (with the idealized characteristics typically required in theoretical models) can be defined such that the model and observed circulations match in the domain of interest. The boundary conditions in the current experiments maintain the surface forcing at constant density with a localized source of destabilizing buoyancy at one end [as assumed in models of Hughes and Griffiths (2006) and Hughes et al. (2007), and which is argued therein to model the thermal boundary conditions used in the experiments of Mullarney et al. (2004)]. The destabilizing buoyancy is assumed in the theory to be supplied at a point or line without an accompanying input of volume or momentum. However, the salinity-induced buoyancy forcing

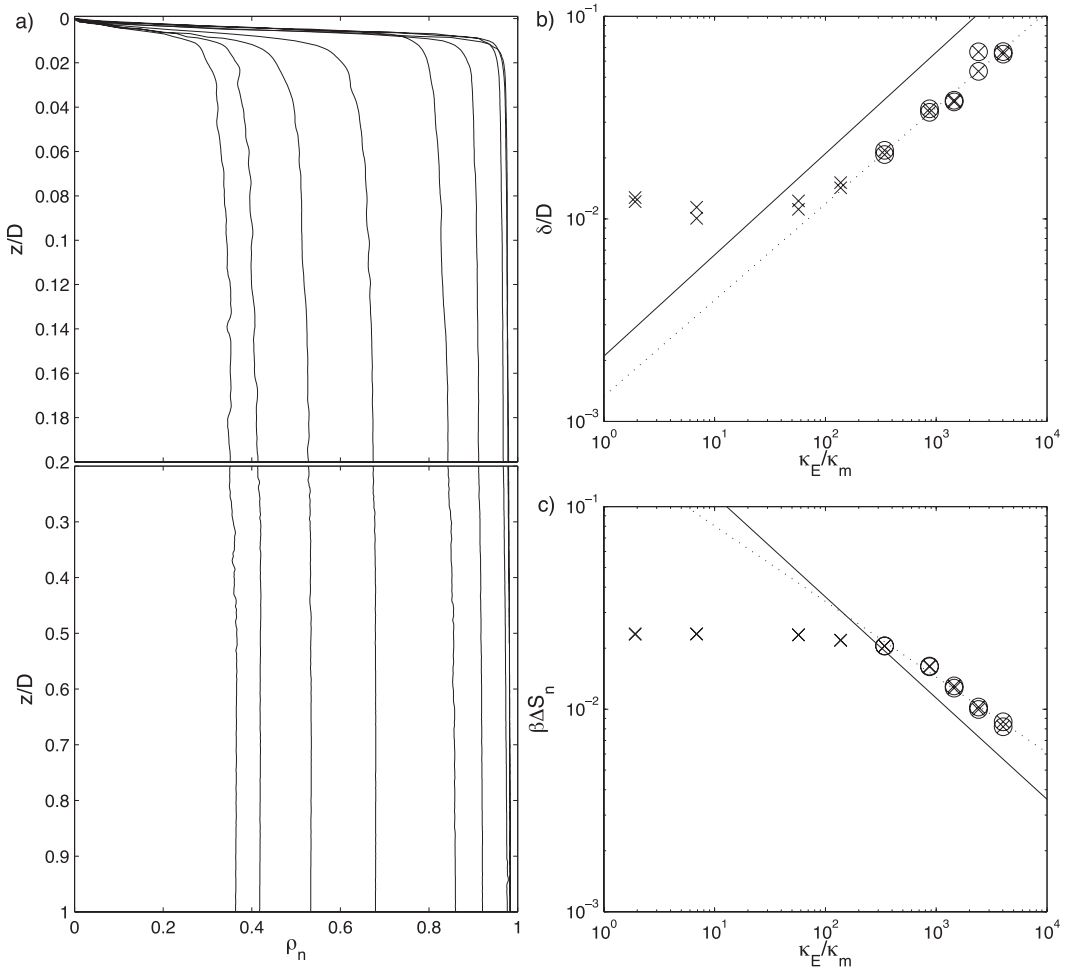

FIG. 4. (a) Vertical profiles of normalized density for expts 1–9; two (virtually coincident) profiles were recorded for each experiment—only one is shown. The rightmost profile is for $\overline{V} = 0$, with increasing $\overline{V}$ to the left. (b),(c) The normalized boundary layer thickness and normalized top-to-bottom salinity difference, respectively, are shown as a function of the externally imposed diffusivity κ_E, normalized by κ_m. The dotted lines depict the least squares fit of the (circled) data in the ''strong stirring'' regime: $\delta/D = 1.3 \times 10^{-3}(\kappa_E/\kappa_m)^{0.475}$ and $\beta\Delta S_n = 0.19(\kappa_E/\kappa_m)^{-0.372}$, respectively. The solid lines are those predicted by the theory of Hughes et al. (2007): $\delta/D = 2.1 \times 10^{-3}(\kappa_*/\kappa_m)^{0.5}$ and $\beta\Delta S_n = 0.36(\kappa_*/\kappa_m)^{-0.5}$, respectively.

in the current experiments impose a maximum salinity and a small, but finite, volume flux across the upper surface. The virtual source correction is made here by assuming the working volume resides within a larger volume with the surface instead at $z = -z_s$ (z is positive downward), where a destabilizing buoyancy flux F_v is imposed by the virtual saline source and the interior density is $\rho(-z_s) = \rho_r (\leq \rho(0) = \rho_f)$. These quantities, which specify the virtual source, are calculated using the theory of Hughes et al. (2007) as outlined in the appendix. Experiments 1–2 and 5–9 are found to lie in different dynamical regimes (termed the ''far-source'' and ''near-source'' limits, respectively), depending on whether the actual source is situated outside or within the stratified virtual boundary layer beneath the virtual source. Experiments 3–4 lie in the transition between these dynamical regimes.

The corrected data and theoretical predictions (Hughes et al. 2007) for normalized boundary layer thickness, top-to-bottom density difference, and streamfunction maxima are plotted in Fig. 6 (note that both the near- and far-source limit corrections are plotted for experiments 3–4 in the transition region). Importantly, the corrected data are all consistent with the predicted scaling dependences upon the rate of irreversible mixing κ_E [Eqs. (7)–(8)]. However, a stronger comparison with the predictions (e.g., evaluating the constant in the power-law relationship) is not possible because the correction procedure is

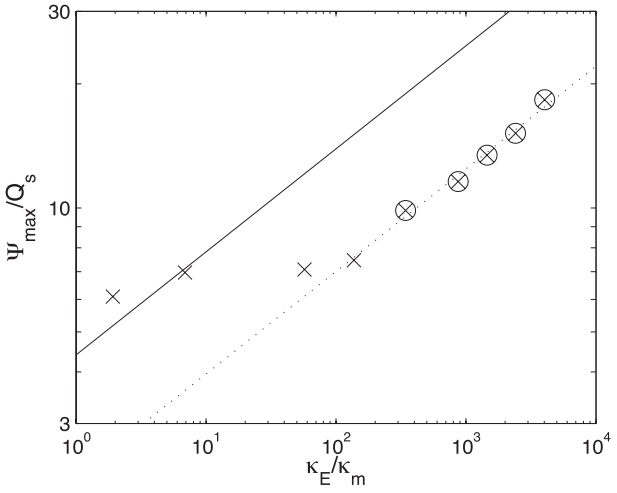

FIG. 5. The maximum volume transport in the plume, normalized by the volume transport of the saline source, as a function of κ_E/κ_m. The dotted line indicates the least squares fit to the (circled) data in the ''strong stirring'' regime: $\psi_{max}/Q_s = 2.2(\kappa_E/\kappa_m)^{0.25}$. The solid line is that predicted by the theory of Hughes et al. (2007): $\psi_{max}/Q_s = 4.4(\kappa_*/\kappa_m)^{0.25}$.

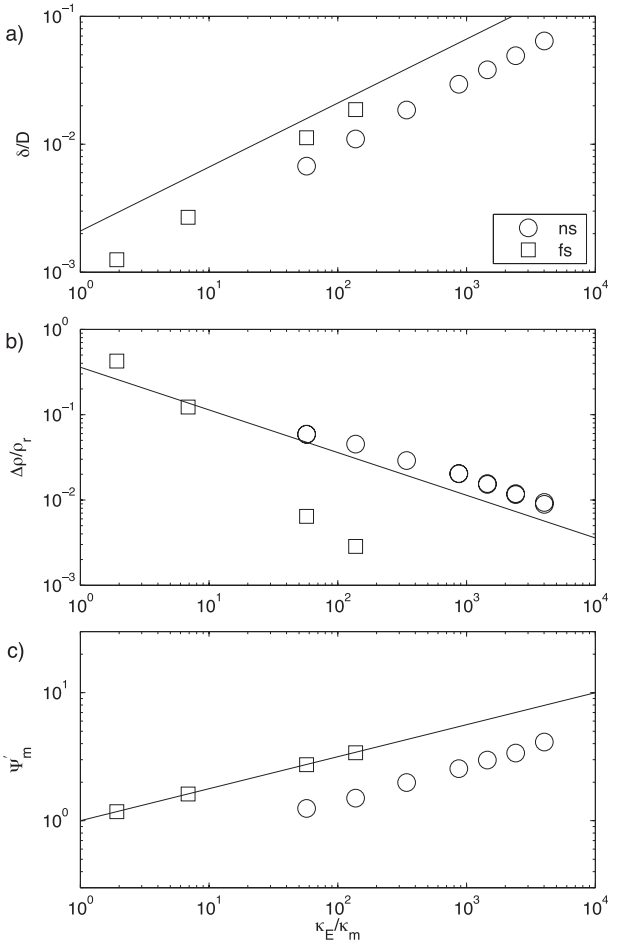

FIG. 6. Summary of experimental data (from Figs. 4 and 5) with the virtual source correction applied (see Appendix) as a function of κ_E/κ_m: (a) normalized boundary layer thickness, (b) normalized top-to-bottom density difference, and (c) normalized streamfunction maxima. Circles and squares indicate data to which the near- and far-source corrections, respectively, were applied; both symbols are shown for experiments in the transition between the two limits. The boundary layer thickness is normalized by the depth of the volume and the top-to-bottom density difference is calculated as $(\rho(D) - \rho_r)/\rho_r$, where $\rho(D)$ is the measured density at the base of the experiment and ρ_r is the reference density at the virtual surface. The streamfunction maxima is normalized using Eq. (4.4) of Hughes et al. (2007) to give $\Psi'_m = \Psi_{max}/(2E^{1/2}D^{1/2}L^{1/4}F_v^{1/4}\kappa_m^{1/4})$, where $E = 0.1$ is the entrainment constant (Turner 1986). The solid lines are those predicted by the theory of Hughes et al. (2007).

itself based on the theory of Hughes et al. (2007); indeed the systematic offset between the near- and far-source streamfunction data arises because the corrections are based on different sets of measurements. The actual and virtual sources have similar characteristics in the strong-stirring regime ($\kappa_E/\kappa_m > 10^2$) because the actual source lies within the stratified boundary layer beneath the virtual source. Conversely, the two sources have very different characteristics in the weak-stirring regime ($\kappa_E/\kappa_m < 10^2$) because the actual source lies beyond the virtual source boundary layer.

The virtual source corrections suggest which physical mechanisms of vertical density transport are important in the flow. The correction calculates idealized boundary conditions in which the surface transport is entirely by diffusion (as in the theoretical models of Hughes and Griffiths 2006; Hughes et al. 2007). Thus we could estimate the corresponding diffusivity as

$$K_v = \frac{\rho_r F_v}{gL(d\rho/dz)|_{z=-z_s}} = \frac{\rho_r F_v \delta_v}{g\Delta\rho_v L}, \qquad (17)$$

based on the properties of the virtual source boundary layer (see appendix): ρF_v is the source buoyancy flux (F_v is the specific buoyancy flux of the source), δ_v is the boundary layer thickness (based on either the near- or far-source limit δ_{ns} and δ_{fs}, respectively), and $\Delta\rho_v = \rho(\delta_v) - \rho_r$ is the density difference across the virtual boundary layer.

In the experiments, conservation of volume in the working volume requires an upward displacement of water at the surface at a rate Q_s. Meanwhile in the steady-state circulation, conservation of salt requires a total mass transport out of the working section at a rate $\rho_s\beta(S_s - S_f)Q_s$ due to both (turbulent) diffusion through the boundary layer and the upward displacement of (relatively fresh) boundary layer water. If the mass transport through the boundary layer was by (turbulent) diffusion alone (as per the idealized theoretical

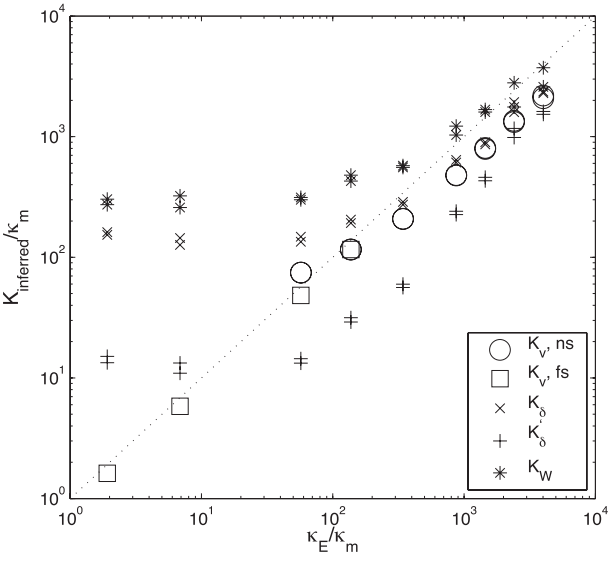

FIG. 7. The parameterized diffusivities, K_v, K_δ, K'_δ, and K_W plotted as functions of the corresponding κ_E and all normalized by κ_m. Circles and squares indicate values of K_v obtained using the near- and far-source corrections, respectively; both symbols are shown for experiments in the transition between the two limits. The dotted line has unity slope and passes through the origin, indicating where the external stirring sets the bulk diffusivity in the experiment.

boundary conditions), we could estimate the required diffusivity [cf. Eq. (17)] as

$$K_\delta = \frac{\rho_s \beta (S_s - S_f) Q_s \delta}{\Delta \rho_\delta L}, \tag{18}$$

where $\Delta\rho_\delta = \rho(\delta) - \rho_f$ is the density difference across the boundary layer. Given the rate of volume displacement from the boundary layer is Q_s, we can also estimate the advective transport of mass through the boundary layer as $M_A = \rho_\delta \beta (S_\delta - S_f) Q_s$, based on the properties of water at the base of the boundary layer (denoted by subscript δ). Thus, if the advective component of transport is explicitly accounted for, the required diffusivity in the boundary layer would be better estimated [cf. Eq. (18)] as

$$K'_\delta = \frac{\beta[\rho_s (S_s - S_f) - \rho_\delta (S_\delta - S_f)] Q_s \delta}{\Delta \rho_\delta L}. \tag{19}$$

The three diffusivity estimates K_v, K_δ, and K'_δ are plotted as a function of κ_E in Fig. 7. It can be seen that the diffusivity inferred from the corrected data is close to the calibrated diffusivity κ_E across all experiments. Thus the virtual source correction shows that the vertical transport through the boundary layer is primarily by (turbulent) diffusion in the strong-stirring regime ($\kappa_E/\kappa_m > 10^2$), where K_v, K_δ, and K'_δ estimates are consistent. However, the advective component of vertical transport dominates through the flow (but not the virtual boundary layer) in the weak-stirring regime ($\kappa_E/\kappa_m < 10^2$), where values of K_v and K'_δ are both significantly less than values of K_δ. The significance of this result is the more general demonstration that (turbulent) diffusion is important for vertical transport within the stratified boundary layer and that advective transport dominates in the interior of the working volume.

A bulk diffusivity calculated from a one-dimensional advection–diffusion balance (e.g., Munk 1966) has been used commonly to represent vertical transport in the oceans. However, our finding regarding the role in experiments of diffusive transport in the interior raises the important question as to what such a bulk diffusivity represents. Following the procedure of Munk (1966) we calculate the bulk diffusivity K_W for these experiments using

$$w \frac{\partial \rho(z)}{\partial z} = K_W \frac{\partial^2 \rho(z)}{\partial z^2}, \tag{20}$$

where w is a uniform upwelling velocity. We first calculate the ratio K_W/w by fitting an exponential function to the vertical profile of (normalized) density and substituting into (20). The fit yields an excellent approximation to the measured profile in all cases and is insensitive to the domain size (which was approximately one-third of the working volume depth, below the threshold in the surface boundary layer corresponding to 66% of the top-to-bottom density difference). This ratio is then multiplied by w (calculated as the area-averaged upwelling required to balance the measured maximum volume transport in the plume) to give K_W. This quantity (normalized by κ_m) is also plotted as a function of κ_E/κ_m in Fig. 7 and always yields the largest value of any diffusivity estimate examined here. When the externally imposed stirring and turbulent diffusion is strong ($\kappa_E/\kappa_m > 10^2$), all parameterized diffusivity values (K_v, K_δ, K'_δ, and K_W) are seen to be consistent. For $\kappa_E/\kappa_m < 10^2$, K_W/κ_m becomes independent of the external stirring, with a value of approximately 3×10^2; in this instance the salt transport has been shown above (for the Rayleigh and Prandtl numbers and aspect ratio used here) to be dominated by mechanisms other than (turbulent) diffusion. The main such mechanism available is horizontal entrainment into and subsequent vertical advection in the turbulent plume.

To emphasize the role of the plume in vertical transport in the convective circulation, we performed two auxiliary experiments in which the saline source was

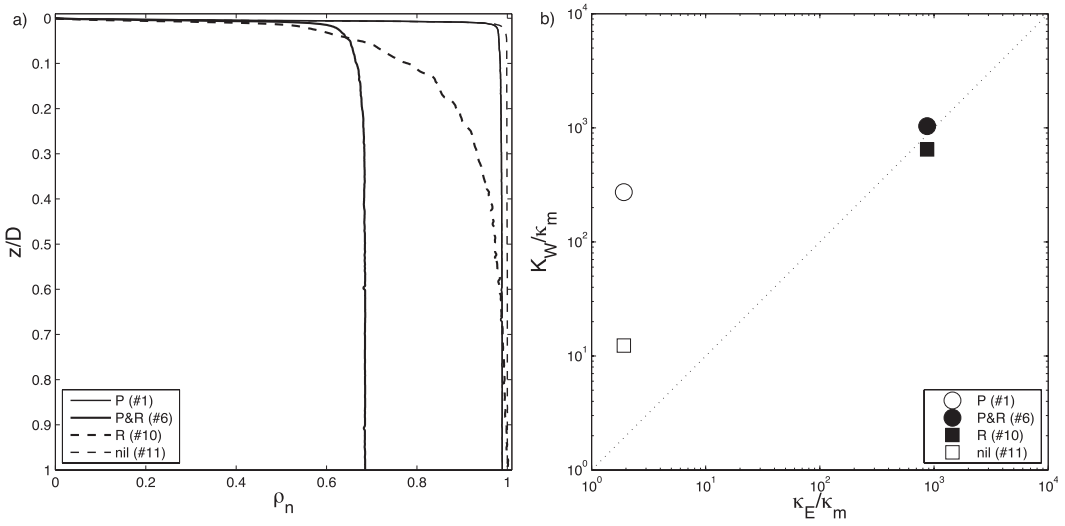

FIG. 8. (a) Vertical profiles of normalized density for expts 1, 6, 10, and 11. The solid and broken lines denote circulations with and without a plume, respectively, and the thicker lines indicate cases with externally imposed stirring. (b) The values of bulk diffusivity inferred by the Munk balance for the same experiments are shown. For large κ_E the presence of a plume has little influence on K_W, indicating that the external stirring sets the total vertical transport; this is not the case for small κ_E.

simply relocated to the bottom left-hand corner of the tank. The source density and volume flux was the same as in the previous experiments, but the turbulent plume was eliminated from the circulation. This configuration removed all convection and any small-scale instabilities, stirring, and associated irreversible mixing that may have been present in the previous experiments. In essence, the auxiliary experiments model the upwelling or interior leg of an overturning circulation without requiring closure by a sinking leg, similar to the implicit assumption used in early attempts to evaluate the vertical diffusivity and interior upwelling velocity in the ocean (Munk 1966). The auxiliary experiments were again run for many filling time scales, once with no added mechanical stirring (experiment 10) and once with added stirring (experiment 11) in the midrange of the κ_E values used for the convection experiments.

The normalized density profiles for the large-time state in the auxiliary experiments are contrasted to the corresponding runs with the source at the surface (experiments 1 and 6) in Fig. 8a. The relevant observation here is that $\rho_n(D) < 1$ for the experiments with the saline source at the surface, whereas $\rho_n(D) = 1$ for experiments with the source at the bottom (i.e., no plume); a plume is needed to effectively transport density anomalies to large depths. Removing both the turbulent plume and external mixing led to a stronger stratification tightly confined at the surface; waters below this were (relatively) unstratified and at the density of the saline source. The addition of external stirring, in the absence of the plume, deepened the surface boundary layer but did not significantly freshen the waters at large depth. In contrast, the cases having the source at the surface showed that the turbulent plume freshened all of the interior, including the water at the bottom; the plume outflow was always less dense than the saline source. The external stirring in these cases again acted to thicken the boundary layer (albeit by a lesser amount than in the case having no plume), thence increasing the rate of freshwater entrainment by the turbulent plume. It is almost entirely via the plume that near-surface water and buoyancy are transported to larger depths.

In the case of the auxiliary experiments, the saline source at the bottom introduces dense water at a rate that is equal to the sum of the upward mass transports by advection and by diffusion at any given level above. The upwelling velocity w is independent of depth and is readily calculated from the volume flux of the saline source and horizontal area of the working volume. The bulk diffusivity in the auxiliary experiments, whether molecular or dominated by the external stirring, is also independent of depth and can be explicitly evaluated by the "Munk balance" in (20). In contrast, when the source is at the surface, entrainment into the turbulent plume ensures that the (horizontally averaged) upwelling in the interior increases with depth. Hence, the Munk procedure (which is based on the maximum overturning transport) will yield a larger bulk diffusivity than would be found using the average rate of upwelling at shallower depths or in the surface boundary layer.

The values of K_W obtained by applying the Munk procedure for experiments 1, 6, 10, and 11 are plotted against the calibrated external mixing rate κ_E in Fig. 8b, again normalized by κ_m. For large κ_E/κ_m the mixing induced by the stirring rods provided the dominant contribution to the vertical transport, whether or not there was a plume, and therefore the inferred diffusivities obtained with the saline source at the bottom and at the surface are similar. However, for no external stirring [$\kappa_E/\kappa_m \sim O(1)$] there is a factor of approximately 30 between the two values of K_W: hence the plume transport very substantially enhanced the inferred value of mixing (note that K_W in the auxiliary experiment without a plume is still greater than κ_E in the case having no external stirring, presumably due to fluid motions induced by the sources). We conclude that depth-dependent vertical transport in the convective overturning circulation, associated with entrainment into the plume (recall that $\Psi_{\max}$ is at least six times larger than Q_s) can cause the diffusivity evaluated by the Munk balance to be significantly larger than in reality, as predicted by Hughes and Griffiths (2006).

A closely related question is whether vertical transport of density anomalies in the global ocean circulation might be dominated by internal processes associated with the overturning or by mixing induced through external means. The laboratory experiments and previous studies provide some guidance. However, we have not varied the molecular diffusivity experimentally, and it is not possible to conclude that the rates of irreversible mixing in the oceans scale with the molecular diffusivity. Nor have we shown systematically what portion of the total vertical transport is due to irreversible mixing (i.e., that excluding advective transport associated with the plume) and how it might depend upon parameters such as basin geometry. Nevertheless, the oceans have an inferred bulk diffusivity $K_W/\kappa_m \sim 10^3$ [evaluated from the Munk (1966) analysis at depths below 1000 m and taking $\kappa_m = 10^{-7}$ m^2 s^{-1} for heat and $K_W \sim 10^{-4}$ m^2 s^{-4}]. When the contribution to the overall vertical transport from the internal process of entrainment into sinking regions and subsequent vertical advection is made explicit, the irreversible mixing characterized by $\kappa_* \sim 10^{-5}$ m^2 s^{-1} (i.e., $\kappa_*/\kappa_m \sim 10^2$) has been shown to be sufficient to explain the observed top-to-bottom density difference and overturning rate of the ocean (Hughes and Griffiths 2006): this is consistent with the measured global average mixing rate of $\kappa_* \approx 1 \times 10^{-5}$ m^2 s^{-1} (Toole et al. 1994; Polzin et al. 1997). Indeed, an order of magnitude difference between K_W and κ_* (or κ_E) owing to the effect of advective plume transport is also consistent with the experimental data (Fig. 8b). However, the relative contributions from the circulation and from external means to irreversible mixing in the interior remains an open and interesting question.

6. Conclusions

The laboratory experiments reported here examine the overturning circulation forced by differential surface buoyancy fluxes and subjected to an imposed level of mechanical stirring. Sources of saline and freshwater provided the buoyancy forcing, and a pair of traversing horizontal rods provided a controlled and calibrated rate of irreversible mixing throughout the circulation. The resulting flow resembled that observed previously in studies of buoyancy-driven overturning circulations.

The measurements (after a virtual source correction in the case of the weaker mixing rates) support the theoretical predictions of Hughes et al. (2007) for the dependence of the density field and circulation on the rate of mixing. In particular, the boundary layer thickness increases with $\kappa_E^{1/2}$, the top-to-bottom density difference decreases with $\kappa_E^{-1/2}$, and the maximum overturning transport increases with $\kappa_E^{1/4}$. Here κ_E is a turbulent diffusivity representing the rate of irreversible mixing of the density field due to both molecular diffusion (down the mean gradient) and that promoted by stirring. The contribution associated with stirring will typically dominate κ_E and is supported by sources of additional kinetic energy external to the circulation itself.

Differences between the boundary conditions achievable in experiments and those idealized in theories conveniently highlight the mechanisms contributing to vertical transport of density in the overturning circulation. The experimental behavior here was determined by the level where the buoyancy forcing was applied relative to that (virtual) level effectively felt by the resulting circulation. When the difference between these two levels was small, (turbulent) diffusion determined the transport of density through the stratified boundary layer formed below the surface. However, when the forcing was in effect applied below the virtual boundary layer (i.e., in the interior), the vertical transport of density is, instead, determined by advective processes. This result can be generalized to delineate regions in an idealized buoyancy-driven overturning circulation; we conclude that diffusive transport processes are important in the strongly stratified surface boundary layer and that advective transport processes dominate below this.

The turbulent plume in large Rayleigh number overturning circulations is the dominant mechanism of vertical transport in the interior. Entrainment of less dense water occurs at all depths, giving rapid advective transport of density anomalies to the bottom and thorough recirculation at depth. Moreover, there is a strong

coupling between the surface boundary layer and the interior—external stirring acts to deepen the boundary layer by enhancing downward mixing of freshwater from the surface. This also leads to a greater buoyancy (at a given level) driving the dense plume. Both of these changes lead to greater entrainment of freshwater into the plume and a smaller top-to-bottom density difference (Hughes and Griffiths 2006). Parameterizations [such as that based on a one-dimensional advection–diffusion balance, Munk (1966)] overlook the details of these vertical transport mechanisms and can lead to bulk diffusivity values well in excess of that which actually characterizes irreversible mixing in the circulation.

The experimental results point to important dynamics in the meridional overturning circulation of the oceans, specifically irreversible mixing in the thermocline and entrainment into the sinking regions. Turbulent mixing arising from energy input to the oceans by winds and tides (the external stirring) is expected to deepen the boundary layer (thermocline) beyond what it would otherwise be, thus modifying the upper ocean density. However, turbulent diffusion is a relatively inefficient means of transporting heat to warm the abyssal depths. Instead, the dense sinking overflows and slope currents can entrain the warmth from the thermocline on their way to forming North Atlantic Deep Water and Antarctic Bottom Water. Thus, the density of deep and bottom waters, and the overturning transport, could be determined primarily by entrainment into and vertical advection by the plumes. In this picture, abyssal mixing could play a significantly lesser qualitative role from a global viewpoint than has commonly been suggested. Furthermore, the rate of irreversible mixing at abyssal depths required to explain ocean measurements can be substantially less than that inferred by parameterizations based on the total vertical transport of density.

Acknowledgments. We are grateful to Andy Hogg, Katarzyna Matusik, Kraig Winters, Bill Young, and two anonymous referees for their insightful discussions and helpful comments, and wish to thank Tony Beasley and Ben Tranter for construction of equipment and laboratory assistance. The work was supported by the Australian Research Council (DP0664115, DP1094542) and GOH was funded by an Australian Research Council Future Fellowship (FT100100869).

APPENDIX

Virtual Source Corrections

The experimentally observed flow is equivalent to the flow that would result from an idealized (''virtual'') line source of buoyancy alone. The virtual source can be specified by (i) the level $z = -z_s$ to which the domain must be extended (in a theoretical sense) above the actual source level at $z = 0$, (ii) the specific buoyancy flux of the virtual source F_v, and (iii) the density that the interior would have at the level of the virtual source $\rho(-z_s)$. Taking the height of both the actual salt source and the freshwater interface to coincide at $z = 0$, the interior density $\rho(0) = \rho_f$, the specific buoyancy flux of the actual salt source $F(0) = gQ_s(\rho - \rho_f)/\rho_r = B\rho_f/\rho_r$, and the horizontally averaged upwelling velocity $w(0) = Q_s/L$. We use the theory of Hughes et al. (2007) to solve for the virtual source, for which it is convenient to define the reference density $\rho_r = \rho(-z_s)$. Relatively simple asymptotic expansions of the full solution yield an accurate approximation to the virtual source when the actual salt source is situated either inside or outside the boundary layer that would be associated with the virtual source.

a. Salt source inside a virtual boundary layer

We assume a priori that the salt source at $z = 0$ lies in the virtual boundary layer of thickness $\delta_{\rm ns}$, that is, $-z_s + \delta_{\rm ns} > 0$. The dimensionless near-source asymptotic approximations for upwelling velocity, buoyancy flux, and interior density [Eqs. (3.3)–(3.5) from Hughes et al. (2007)] are formally valid if $(1 - F(0)/F_v) \ll 1$. Combining these approximations with the expressions above for $F(0)$ and $w(0)$ and Eqs. (2.15), (2.18), and (2.20) from Hughes et al. (2007), we can write

$$z_s = 2^{-1/3}E^{-2/3}F_v^{-1/3}Q_s, \tag{A1}$$

$$F(0) \approx F_v \exp(-2^{-4/3}E^{-2/3}F_v^{-1/3}\kappa_E^{-1}L^{-1}Q_s^2), \tag{A2}$$

and, retaining only the first two terms of the error function series expansion,

$$\frac{g(\rho_r - \rho_f)}{\rho_r} \approx -F_v\kappa_E^{-1}L^{-1}z_s \times [1 - 2^{-2/3}3^{-1}E^{2/3}F_v^{1/3}\kappa_E^{-1}L^{-1}z_s^2]. \tag{A3}$$

Here $E = 0.1$ is the entrainment coefficient characterizing a turbulent plume (e.g., Turner 1986). This system of equations is solved to give z_s, F_v, and $\rho_r = \rho(-z_s)$ given the known values of Q_s, κ_E, and B. The calculation also gives the virtual boundary layer scale

$$\delta_{ns} = 2^{-1/6}E^{-1/3}F_v^{-1/6}\kappa_E^{1/2}L^{1/2}, \tag{A4}$$

and the near-source approximation is expected to hold for $z_s \lesssim \delta_{\rm ns}$ (see Fig. 3 of Hughes et al. 2007).

b. Salt source outside the virtual boundary layer

A ''far source'' asymptotic approximation can be used to find the virtual source if the salt source lies well outside the virtual boundary layer. The interior density and buoyancy flux are a weak function of height, and the measured maximum overturning transport in the plume $\Psi_{\max} \approx w(D)L$ ($m^2\ s^{-1}$) is instead used to accurately calculate the virtual source. Equations (2.15) and (2.18) and the far-source approximations for dimensionless upwelling velocity and top-to-bottom density difference in the interior from Table 1 of Hughes et al. can be manipulated to give

$$F_v = \frac{(\Psi_{\max}^2 - Q_s^2)^2}{16E^2\kappa_E LD^2}, \tag{A5}$$

$$z_s = 2^{-1/6}E^{-1/3}F_v^{-1/6}(\kappa_E L)^{1/2} \times [0.903 + 2^{-11/6}E^{-2/3}F_v^{-1/3}\kappa_E^{-1}L^{-1}Q_s^2], \tag{A6}$$

$$\frac{g[\rho_r - \rho(D)]}{\rho_r} = -1.28 \times 2^{-1/6}E^{-1/3}F_v^{5/6}\kappa_E^{-1/2}L^{-1/2}. \tag{A7}$$

The corresponding boundary layer scale δ_{fs} is given by substituting the far-source value of F_v into Eq. (A4); the far-source approximation is expected to hold for $z_s \gtrsim 4\delta_{\mathrm{fs}}$ (see Fig. 3 of Hughes et al. 2007).

REFERENCES

Bryan, F., 1987: Parameter sensitivity of primitive equation ocean general circulation models. *J. Phys. Oceanogr.,* **17,** 970–985.

Gregg, M. C., 1987: Diapycnal mixing in the thermocline: A review. *J. Geophys. Res.,* **92,** 5249–5286.

Hughes, G. O., and R. W. Griffiths, 2006: A simple convective model of the global overturning circulation, including effects of entrainment into sinking regions. *Ocean Modell.,* **12,** 46–79.

——, and ——, 2008: Horizontal convection. *Annu. Rev. Fluid Mech.,* **40,** 185–208.

——, ——, J. C. Mullarney, and W. H. Peterson, 2007: A theoretical model for horizontal convection at high Rayleigh number. *J. Fluid Mech.,* **581,** 251–276.

——, A. McC. Hogg, and R. W. Griffiths, 2009: Available potential energy and irreversible mixing in the meridional overturning circulation. *J. Phys. Oceanogr.,* **39,** 3130–3146.

Kuhlbrodt, T., A. Griesel, M. Montoya, A. Levermann, M. Hofmann and S. Rahmstorf, 2007: On the driving processes of the Atlantic meridional overturning circulation. *Rev. Geophys.,* **45,** RG2001, doi:10.1029/2004RG000166.

Mullarney, J. C., R. W. Griffiths, and G. O. Hughes, 2004: Convection driven by differential heating at a horizontal boundary. *J. Fluid Mech.,* **516,** 181–209.

Munk, W. H., 1966: Abyssal recipes. *Deep-Sea Res.,* **13,** 707–730.

——, and C. Wunsch, 1998: Abyssal recipes II: Energetics of tidal and wind mixing. *Deep-Sea Res.,* **45,** 1976–2009.

Paparella, F., and W. R. Young, 2002: Horizontal convection is non-turbulent. *J. Fluid Mech.,* **466,** 205–214.

Pierce, D. W., and P. B. Rhines, 1996: Convective building of a pycnocline: Laboratory experiments. *J. Phys. Oceanogr.,* **26,** 176–190.

Polzin, K. L., J. M. Toole, J. R. Ledwell, and R. W. Schmitt, 1997: Spatial variability of turbulent mixing in the abyssal ocean. *Science,* **276,** 93–96.

Rossby, H. T., 1965: On thermal convection driven by non-uniform heating from below: An experimental study. *Deep-Sea Res.,* **12,** 9–16.

Ruddick, B. R., and T. G. L. Shirtcliffe, 1979: Data for double diffusers: Physical properties of aqueous salt-sugar solutions. *Deep-Sea Res.,* **26A,** 775–787.

Scotti, A., and B. White, 2011: Is horizontal convection really ''non-turbulent''? *Geophys. Res. Lett.,* **38,** L21609, doi:10.1029/2011GL049701.

Toole, J. M., K. L. Polzin, and R. W. Schmitt, 1994: Estimates of diapycnal mixing in the abyssal ocean. *Science,* **264,** 1120–1123.

Tsujino, H., H. Hasumi, and N. Suginohara, 2000: Deep Pacific circulation controlled by vertical diffusivity at the lower thermocline depths. *J. Phys. Oceanogr.,* **30,** 2853–2865.

Turner, J. S., 1986: Turbulent entrainment: the development of the entrainment assumption, and its application in geophysical flows. *J. Fluid Mech.,* **173,** 431–471.

Washburn, E. W., Ed., 2003: *International Critical Tables of Numerical Data, Physics, Chemistry and Technology.* Knovel, 507 pp.

Whitehead, J. A., and W. Wang, 2008: A laboratory model of vertical ocean circulation driven by mixing. *J. Phys. Oceanogr.,* **38,** 1091–1106.

Wunsch, C., and R. Ferrari, 2004: Vertical mixing, energy, and the general circulation of the oceans. *Annu. Rev. Fluid Mech.,* **36,** 281–314.